HHS Public Access

Author manuscript

Int J Cancer. Author manuscript; available in PMC 2016 November 15.

Published in final edited form as:

Int J Cancer. 2015 November 15; 137(10): 2403–2412. doi:10.1002/ijc.29611.

A quantitative microscopic approach to predict local recurrence based on *in vivo* intraoperative imaging of sarcoma tumor margins

Jenna L. Mueller[1,*], **Henry L. Fu**[1], **Jeffrey K. Mito**[2], **Melodi J. Whitley**[2], **Rhea Chitalia**[1], **Alaattin Erkanli**[3], **Leslie Dodd**[4], **Diana M. Cardona**[5], **Joseph Geradts**[5], **Rebecca M. Willett**[6], **David G. Kirsch**[2,7], and **Nimmi Ramanujam**[1]

[1]Department of Biomedical Engineering, Duke University, Durham, North Carolina, USA

[2]Department of Pharmacology & Cancer Biology, Duke University School of Medicine, Durham, North Carolina, USA

[3]Department of Biostatistics & Bioinformatics, Duke University, Durham, North Carolina, USA

[4]Department of Pathology, University of North Carolina School of Medicine, Chapel Hill, North Carolina, USA

[5]Department of Pathology, Duke University Medical Center, Durham, North Carolina, USA

[6]Department of Electrical and Computer Engineering, University of Wisconsin - Madison, Madison, Wisconsin, USA

[7]Department of Radiation Oncology, Duke University School of Medicine, Durham, North Carolina, USA

Abstract

The goal of resection of soft tissue sarcomas located in the extremity is to preserve limb function while completely excising the tumor with a margin of normal tissue. With surgery alone, one-third of patients with soft tissue sarcoma of the extremity will have local recurrence due to microscopic residual disease in the tumor bed. Currently, a limited number of intraoperative pathology-based techniques are used to assess margin status; however, few have been widely adopted due to sampling error and time constraints. To aid in intraoperative diagnosis, we developed a quantitative optical microscopy toolbox, which includes acriflavine staining, fluorescence microscopy, and analytic techniques called sparse component analysis and circle transform to yield quantitative diagnosis of tumor margins. A series of variables were quantified from images of resected primary sarcomas and used to optimize a multivariate model. The sensitivity and specificity for differentiating positive from negative *ex vivo* resected tumor margins was 82% and 75%. The utility of this approach was tested by imaging the *in vivo* tumor cavities from 34 mice

[*]Corresponding author: Jenna L. Mueller, Duke University, 136 Hudson Hall Box 90281, Durham, NC 27708, Phone: 919-660-8473, Fax: 919-684-4488, jenna.mueller@duke.edu.

Financial disclosures: Dr. Ramanujam has founded a company called Zenalux Biomedical and she and other team members have developed technologies related to this work where the investigators or Duke may benefit financially if this system is sold commercially. Dr. Kirsch is on the scientific advisory board for Lumicell Inc., which is commercializing intraoperative imaging technology.

after resection of a sarcoma with local recurrence as a bench mark. When applied prospectively to images from the tumor cavity, the sensitivity and specificity for differentiating local recurrence was 78% and 82%. For comparison, if pathology was used to predict local recurrence in this data set, it would achieve a sensitivity of 29% and a specificity of 71%. These results indicate a robust approach for detecting microscopic residual disease, which is an effective predictor of local recurrence.

Keywords

Optical fluorescence imaging; Intraoperative imaging; Soft Tissue Sarcoma; Image analysis; Logistic models

INTRODUCTION

The goal of resection of soft tissue sarcomas located in the extremity is to completely excise the tumor while preserving limb function. Typically, the completeness of the excision is determined by pathologic assessment several days after surgery. Positive margin status, which is indicated by the presence of tumor cells at the edge of the resected specimen, has been reported to correlate with local recurrence, development of metastasis, and overall survival [1–3]. In the absence of adjuvant radiation therapy, microscopic disease left at the surgical site causes local recurrence in up to 31% of sarcoma patients [2, 4]. While intraoperative techniques, such as touch prep cytology and frozen section analysis, have been used to assess margins during surgery, these techniques require laboratory personnel to be present at the time of surgery [5, 6]. Additionally, due to time constraints these techniques can only sample 1 or 2 small regions of the margin, which can result in significant sampling error. Taken together, there exists an opportunity to improve intraoperative assessment of tumor margins.

Microscopy is a powerful technique that can provide intraoperative visualization of excised margins as well as the tumor cavity. Various microscopy techniques including reflectance and fluorescence [7, 8], confocal [9, 10], and optical coherence tomography [11, 12] have been used to visualize micro-anatomic tissues at the point of care, similar to what a pathologist visualizes when looking at tissue sections.

Previously, our group used a high resolution fluorescence microendoscope in combination with a topical contrast agent called acriflavine, which binds to nucleic acids, to enable visualization of the microanatomical features in resected tumor surgical margins [13]. This study was carried out using genetically engineered mice with conditional mutations in *p53* and either *K-ras* or *B-raf* after they developed primary sarcomas [14, 15]. A primary sarcoma model was chosen because it more closely mimics the tumor invasion into adjacent skeletal muscle found in human sarcomas as compared to xenograft models. We developed a strategy for isolating acriflavine positive features (APFs) from the heterogeneous sarcoma margins, using a technique called sparse component analysis (SCA) [13], which has been used in the image processing community for image compression, enhancement, and restoration. SCA accurately isolated APFs from images of excised tumor, muscle, adipose, and tumor +

muscle tissues, and differences in both density and size could be leveraged to identify pathologically confirmed positive images [13].

The goal of our current study was to test the robustness of our quantitative microscopy tool box to predict local recurrence based on the presence of residual sarcoma cells in the resection cavity of genetically engineered mice. Specifically, we aimed to determine if variables, such as the density and size of APFs, could be used to develop a diagnostic model that detects the presence of microscopic residual disease. To meet this goal, a logistic regression model was optimized on resected tissue sites and prospectively applied to the panel of images obtained from the tumor cavity of 34 mice. After surgery, the mice were monitored for local recurrence, and the results from our diagnostic model were compared to local recurrence endpoints.

MATERIAL AND METHODS

Sarcoma generation

Temporally and spatially restricted primary sarcomas were induced as described previously by Kirsch et al [14]. Briefly, mice with conditional mutations in *p53* and either oncogenic *K-ras* or *B-raf* [15] were injected with an adenovirus expressing Cre-recombinase, and palpable tumors could be detected approximately 30–60 days later. Sarcomas were excised as described by Mito et al [16]. The protocol was approved by the Duke University Institutional Animal Care and Use Committee.

Imaging system and contrast agent

A high resolution fluorescence microendoscope that has been described previously [17] was used to capture images of sarcoma margins. Briefly, the microendoscope contained a 455 nm light emitting diode, excitation filter, dichroic mirror, 10x objective, emission filter, and CCD camera. The light was directed to the sample through a flexible fiber bundle that yielded a circular field of view of 750 μm in diameter and a resolution of 4.4 μm. The system was used with a contrast agent called acriflavine, which reversibly associates with nucleic acids, such as RNA and DNA, and has also been shown to stain muscle fibers and collagen [18, 19]. Acriflavine was dissolved in phosphate buffered saline solution (0.01% w/v, Sigma-Aldrich) and was topically applied to the tissue immediately before placing the fiber bundle in contact with the tissue and acquiring images.

Ex vivo imaging protocol

A total of 6 mice were included in the *ex vivo* study. Excised tissue sections were laid flat and 3 to 5 drops of acriflavine were topically applied. Within 30 seconds of applying acriflavine, the fiber probe was placed into contact with the tissue and images were taken from 3 to 5 sites per specimen. Each site was inked with a 1 mm dot for pathological diagnosis. *En face* or tangential sections were cut from directly below each dot and submitted for H&E processing. Each dot was reviewed by two pathologists and given a diagnosis of tumor, muscle, tumor + muscle (T+M), or adipose. Only sites for which the diagnosis was concordant between the two pathologists (n= 27 of 33 sites) were included in subsequent analysis.

In vivo imaging protocol

A total of 34 mice were included in the *in vivo* study. Tumors located on the lower hind limbs of mice were surgically excised. 3 to 5 drops of acriflavine were topically applied to the tumor cavity, and the fiber probe was placed in contact with the tissue. The probe was raster scanned in 1 mm increments in order to create a mosaic of the *in vivo* margin. Mosaics varied from 3 × 3 images up to 5 × 4 or 4 × 5 images depending on the size of the tumor cavity. After imaging, the excised margin that mirrored the *in vivo* tumor cavity was inked and submitted for H&E processing. The excised margins were sectioned tangentially (*en face*) and the three most superficial sections were given separately to two pathologists for diagnosis. If there were tumor cells present in any of the sections, the margin was diagnosed as positive (Path+). If there were no tumor cells, the margin was diagnosed as negative (Path −). Only margins for which there was a concordant positive or negative pathology diagnosis between the two pathologists were labeled as Path+ or Path−. Mice with discordant pathology were labeled as Path N/A. Additionally, mice were followed for local recurrence for up to 200 days. The 200 day mark was selected because it was approximately twice the length of the latest recurrence in an initial cohort of mice [16]. If a palpable mass could be detected within 200 days, then the tumor locally recurred. If no palpable mass was detected after 200 days, then the tumor did not locally recur. If the mouse did not survive for 200 days post-surgery, then no local recurrence endpoint was achieved.

Sparse component analysis (SCA) for AFP segmentation

All image processing and analysis was completed in MATLAB (2013b, Mathworks Inc., Natick, MA). APFs were segmented by applying a technique called sparse component analysis (SCA), which has been described previously [13]. Briefly, SCA is a computational technique that leverages the morphological information present in the fluorescent images of acriflavine stained microanatomy and separates distinct structures into mathematically discrete components. SCA was used here to separate APFs from muscle and adipose structures in heterogeneous images.

After SCA was applied to isolate AFPs, variables such as the size and density were quantified by computing the circle transform [20] (CT) to detect approximately circular objects, which could represent nuclei. CT was chosen to quantify variables because it can distinguish overlapping circular AFPs and is easy to tune.

Calculation of AFP variables

AFP variables were designed to capture features that pathologists typically use to distinguish between normal and diseased tissue. Diseased features typically include increased nuclear density with aneuploidy and pleomorphism (the variation in size and shape of nuclei) [21, 22]. Specifically AFP variables include density, which is the number of AFPs in a specified area, and diameter, which is defined as the diameter given by the output of CT.

Model development with *ex vivo* data set

In order to develop a model to distinguish between positive and negative *in vivo* margins, the *ex vivo* data set was used to examine trends corresponding to the pathology diagnosis.

First, Wilcoxon rank sums (non-parametric, two-tailed, alpha = 0.05) were used to determine whether quantitative image parameters were significantly different between positive and negative images. Next, a multivariate variable-selection analysis based on logistic regression in SAS programming environment was carried out in which all combinations of variables were initially considered for the *ex vivo* data set. Multivariate logistic regression models yielded receiver operator characteristic curves and the area under the curve for each variable-selection iteration. The area under the curve associated with each model was recorded and tabulated. Additionally, the cross-validated probabilities for each image were determined in SAS using leave one out cross-validation and then used to construct a receiver operator characteristic curve, which was built with a web-based tool [23].

Application of optimized models to the *in vivo* data set

The models that yielded the highest area under the curve for the *ex vivo* data set were directly applied to *in vivo* tumor cavity for which a local recurrence endpoint was obtained. For the *in vivo* tumor cavities, nuclear variables were calculated for the entire panel. The model that yielded the highest area under the curve for the *in vivo* data set was selected. A cut point on the receiver operator characteristic curve was selected based on the objective function $F = (1\text{-sensitivity})^2+(1\text{-specificity})^2$, which is minimized at the optimal cut point.

RESULTS

Optimization of SCA, CT and logistic regression on resected margins

Original images of the resected margins showing tumor, muscle, adipose, or tumor and muscle (T+M) are shown in row 1 of Figure 1A. The images were processed using SCA and individual APFs were quantified with CT. The overlays of SCA+CT are shown in row 2. For the overlay, APFs that were larger than 7 μm in diameter were false colored red and APFs that were less than or equal to 7 μm in diameter were false colored green. The threshold of '7 μm' was chosen because two populations in diameter were observed in the histogram as shown in Figure 1C – one population centered around 5 μm in diameter and one around 10 μm. Furthermore, a threshold of '7 μm' was chosen because approximately 75% of APFs were captured in the less than 7 μm (green) group within the tumor and T+M samples. In previous work, a threshold of '8 μm' was used [13]; however, upon further investigation a threshold of '7 μm' led to more significant differences in density between positive and negative *ex vivo* images. As seen, SCA can be used to isolate APFs in a variety of heterogeneous images with tumor cells demonstrating a much narrower distribution of sizes compared to images of adipose and muscle tissues. Figure 2A–C shows boxplots of density for all APFs, as well as the smaller and larger APFs calculated from tumor (n=8), muscle (n=13), and T+M (n=6) images. As expected, each density boxplot shows a decreasing trend from tumor to T+M to muscle. The density of the smaller APFs (green) yields the most significant differences between malignant and benign images ($p = 0.0016$). Figure 2D shows significantly smaller mean diameters for tumor and T+M compared to muscle ($p = 0.021$).

Multivariate models were constructed using combinations of variables shown in Figure 2. Each density variable was paired with the mean diameter variable. All combinations of variables performed comparably on the training set. The set of variables which had the

smallest difference between the training and cross-validation set were a combination of the density of the smaller APFs (green) and mean diameter.

Prediction of local recurrence using an optimized algorithm based on SCA, CT and logistic regression

The SCA+CT overlays of a representative LR+/Path+ and LR−/Path− margin are shown in Figure 4A and B respectively. The APF diameters from the two margins were quantified using SCA+CT and are shown in Figure 4C. As seen, the distribution of the LR−/Path− margin is slightly shifted to the right, which is similar to the trends seen in Figure 1C. Additionally, large differences in density are present between the two margins; specifically, the LR+/Path+ margin contains 617 total APFs (123 APFs/mm^2) while the LR−/Path− margin contains 141 total APFs (47 APFs/mm^2).

Local recurrence and pathology endpoints for the 34 mouse study are listed in columns 1 and 2 of Table 1. Local recurrence endpoints were achieved for 26 out of 34 mice; the other 8 mice died in post-operative period. Out of the 26 mice where local recurrence could be scored, 9 locally recurred and 17 did not locally recur. Local recurrence and pathology endpoints were not always concordant. Out of the 26 mice that achieved local recurrence endpoints, only 12 (approximately 46%) had matched pathology and local recurrence endpoints—2 mice were LR+/Path+ and 10 were LR−/Path−. For 9 of the 26 mice, the endpoints did not match—5 mice were LR+/Path− and 4 mice were LR−/Path+. The remaining 5 mice that achieved a local recurrence endpoint had discordant pathological diagnosis between the two pathologists. Because of the high degree of discordance, local recurrence was used as the primary endpoint to compare the imaging results.

Next, the multivariate models combining SCA+CT and logistic regression were applied to the *in vivo* local recurrence data set. The receiver operator characteristic curves achieved with each of the models shown in Figure 3 are shown in Figure 5. Density (green) + diameter and density (both) + diameter are the best performing two variable models for the *in vivo* local recurrence data set with an area under the curve for all margins = 0.81 and 0.82, respectively (Figure 5A, B). While the three variable model also achieved an area under the curve = 0.82, no improvement in performance was obtained through adding an additional variable.

The optimal cut point on the density (green) + diameter curve in Figure 5B yielded 7 true positives, 2 false negatives, 14 true negatives, and 3 false positives, resulting in a sensitivity of 78% and a specificity of 82%. For comparison, if pathology was used to predict local recurrence in this data set, it would achieve a sensitivity of 29% and a specificity of 71%. The number of true positives, false negatives, true negatives, and false positives associated with density (green) + diameter that fell within each category is shown in Table 1 columns 3–6. Interestingly, for the 2 (100%) false negatives and 1 out of the 3 (33%) false positives, the imaging correlated with the pathology assessment, but not with local recurrence (LR+/Path− and LR−/Path+). For the other 2 false positives – one had matched pathology (LR−/Path−) and the other had a discordant pathological diagnosis (LR−/Path N/A). For 3 out of the 7 (43%) true positives, the pathology did not match local recurrence (LR+/Path−). In addition, in 4 out of the 14 (29%) true negatives, the pathology did not match local

recurrence (LR−/Path+). For the margins that had matched local recurrence and pathology, 100% of LR+/Path+ margins were correctly classified as true positives by imaging and 90% of LR−/Path− margins were correctly classified as true negatives by imaging.

DISCUSSION

We have demonstrated that our quantitative microscopy toolbox provides a robust approach to identify microscopic residual disease in the *in vivo* tumor cavity. A strength of this method is that it is particularly well suited for applications to different organ sites given that (1) it leverages the micro-anatomical changes in pathological tissue, similar to pathology and (2) it can be applied to highly heterogeneous tissues consisting of multiple tissue types. Moreover, no additional optimization of SCA+CT and logistic regression was required for the algorithm to be effective in analyzing images from the *in vivo* tumor cavity after resection of the sarcomas, suggesting that the features identified by our technology are independent of whether it is applied to excised or intact tissues.

The primary sources of contrast observed in this study were density and diameter. In particular, the density of the smaller APFs and mean diameter achieved the best performance in distinguishing between margins that locally recurred and margins that did not locally recur. As expected, there are higher values of density for images of positive *ex vivo* margins and *in vivo* tumor cavities than for images of negative *ex vivo* margins and *in vivo* tumor cavities. Conversely, there were lower values of mean diameter for positive *ex vivo* margins and *in vivo* tumor cavities than for negative *ex vivo* margins and *in vivo* tumor cavities. This result is consistent with results seen in our previous work [13] and is most likely due to the acriflavine stained nucleic acids being highly concentrated in the nucleoli within sarcoma nuclei, which reduces the average diameter. Conversely, the nucleic acids are more diffuse within muscle and adipose nuclei. Additionally, sarcoma cells are often interspersed with inflammatory cells, such as macrophages and lymphocytes, whose nuclei are typically smaller than sarcoma cell nuclei, which also reduce the average diameter. A separate analysis was conducted on H&E stained slides in which both the major and minor axis of 10 nuclei were quantified by a pathologist (Supplementary Figure 1). While results indicates that sarcoma nuclei are the largest, sarcoma nucleoli, macrophage nucleoli, and lymphocyte nuclei are much smaller and consistent with the size distributions seen in our study. Additionally, SCA+CT is designed to detect objects that are approximately circular; therefore, if an APF is more ellipsoidal, we are likely measuring the minor axis. Based on the bimodal distributions seen in Figure 1, the smaller AFPs primarily correspond to sarcoma nucleoli, macrophage nucleoli, and lymphocyte cell nuclei and the larger AFPs primarily correspond to muscle and adipose nuclei. In summary, the trends from the H&E analysis are reflected in our data—the average diameter of the sarcoma APFs is smaller than the average diameter of muscle and adipose APFs. Lastly, the fact that the best model determined from the *ex vivo* data set—density (green) + diameter yielded the highest performance when applied to the *in vivo* data set shows consistency between *ex vivo* and *in vivo* imaging, which suggests that *ex vivo* imaging can be a good surrogate for *in vivo* imaging when *in vivo* imaging is not clinically feasible.

Similar to human soft tissue sarcomas [2, 4], we found that local recurrence and pathology of the resected margins for mouse sarcomas do not always match. Therefore, in our study we compared imaging results to local recurrence and pathology separately. In a separate cohort of 25 mice that had resection of a primary sarcoma on which only histological margin assessment was performed (i.e. no imaging), no significant difference in the rate of local recurrence was observed for mice with either a negative or positive margin diagnosis (Supplementary Figure 2). Possible reasons for the discrepancy between margin status and local recurrence include the limitations and potential errors associated with the pathologic assessment. For example, the ink used to delineate the excised tissue margin can run into crevices where it does not belong, either of which could yield incorrect results. Moreover, it is possible that residual tumor cells (positive margin) are eliminated by the post-surgical inflammatory response or cautery effect on the tumor, thus preventing growth of a local recurrence. Additionally, tumor deposits are not necessarily continuous and can migrate resulting in 'skip lesions', which may not be detected. Lastly, *en face*/tangential sectioning of the excised tissue margin was chosen for this study to assess the superficial area of the excised tumor that mirrored the *in vivo* tumor cavity and imaged surface; however, perpendicular sectioning is traditionally done in clinical settings, which may ultimately better correlate with local recurrence. Due to these possible sources of error associated with pathology and the ultimate clinical importance, local recurrence was used as the endpoint on which to compare our imaging technique. Importantly, when local recurrence and pathology endpoints matched, there was an additional degree of concordance with imaging; 100% of LR+/Path+ margins were correctly classified as true positives by imaging and 90% of LR−/Path− margins were correctly classified as true negatives by imaging. This increased performance may correlate with the tumor volume left behind – specifically for LR+/Path+ margins, there may be a large amount of tumor present on the excised margin as well as in the *in vivo* tumor cavity.

The primary challenge with this technique is the field of view (FOV). While it is feasible to create mosaics by scanning a sarcoma tumor bed in a mouse, which is on the order of 3–7 mm in any one dimension, it is not feasible to evaluate an entire human surgical margin. We foresee that high resolution anatomical imaging could be combined with wide-field devices, such as a device that we have utilized to detect protease-activated fluorescent imaging agents [16, 24]. Specifically, the wide-field imaging device has a 9.0 × 6.6 mm (59.4 mm^2) FOV and has been used to intraoperatively detect residual tumor after wide resections of soft tissue sarcoma in 9 dogs [16, 24]. Additionally, improvements to the microscopic imaging system could also be made to increase the FOV while maintaining the sub-cellular resolution needed for delineation of nucleoli. One approach is to employ a technique called structured illumination microscopy (SIM), where the entire FOV is illuminated with a defined spatial pattern rather than scanning a focal spot, such as in confocal microscopy [25]. Towards this end, we have developed a wide-field fluorescence SIM system with a FOV of 2.1×1.6 mm (3.4 mm^2) and sub-cellular resolution (4.4 μm) [26].

This study was conducted in a preclinical sarcoma model in order to assess whether a combination of imaging tools could detect residual disease in resected tumor cavities. Moving forward, our goal is to expand this work to tumor margin assessment in humans.

The high resolution fluorescent microscope used in this study is a non-significant risk device. The device emits light into the tissue and with the use of acriflavine provides high resolution images of the tissue. Acriflavine (also commonly referred to as proflavine) is a topical antiseptic that has been safely used for years as one of the main components of triple dye, which is applied to the umbilicus of newborns to prevent infection [27, 28]. Acriflavine has also been routinely used as an antibacterial agent and was employed as a wound disinfectant during World War I [29]. Additionally, acriflavine has been topically applied *in vivo* to both the oral mucosa and cervix and imaged with a microendoscope by several groups [17, 30–32]. No adverse events or *in vivo* side-effects were reported in these studies. According to safety information from Sigma-Aldrich, the acute toxicity of acriflavine is 1,048 mg/kg of body weight (no dilution), and no component of the product present at levels greater than or equal to 0.1% is identified as a carcinogen or potential carcinogen [33]. We selected a concentration of 0.01% for this study because it was 10 fold below the 0.1% threshold, but was still sufficiently bright to stain and image tissue morphology. We applied 3–5 drops (0.15–0.25 mLs) to the resection cavities because that volume was sufficient to cover the entire cavity, which was approximately 7 × 7 mm (49 mm^2) or smaller. If extended to humans, 5 drops would be needed per approximately 50 mm^2. At a concentration of 0.01%, acriflavine costs approximately one hundredth of a cent per mL [33]. The high resolution fluorescent microscope can be built from off the shelf components for a total cost of $2,500 [17]. Thus, this approach could potentially provide a low cost tool for intraoperative assessment of tumor margins.

In conclusion, we have combined topical acriflavine staining and high resolution microscopy with appropriate strategies for segmentation and selection of APFs for automated detection of microscopic residual sarcoma *in vivo*. This combination of technologies could be particularly useful in deconstructing images of heterogeneous tissues and could easily be combined with other wide-field imaging platforms for clinical use. Ultimately, this study demonstrates that morphological surveillance of tissue can be leveraged for detection of residual disease on tumor margins *in vivo* and presents a framework for intraoperative imaging and analysis that could be applied to a variety of different tissues.

Supplementary Material

Refer to Web version on PubMed Central for supplementary material.

Acknowledgments

The project described was supported by the Department of Defense Grant Number W81XWH-09-1-0410 and the NIH Grant Number 1R01EB01157.

We thank Dr. Rebecca Richards-Kortum and her student, Jessica Dobbs, for providing the imaging system and guidance on image acquisition. We thank several investigators for providing mice: Dr. Tyler Jacks for conditional K-ras mutant mice, Martin McMahon for conditional B-raf mutant mice, and Dr. Anton Berns for conditional p53 mutant mice.

Abbreviations used

APFs	acriflavine positive features
SCA	sparse component analysis
CT	circle transform
LR+/Path+	locally recurred and pathologically positive
LR+/Path−	locally recurred and pathologically negative
LR+/Path N/A	locally recurred and discordant pathology
LR−/Path−	recurrence free and pathologically negative
LR−/Path+	recurrence free and pathologically positive
LR−/Path N/A	recurrence free and discordant pathology

References

1. Lewis JJ, Leung D, Casper ES, Woodruff J, Hajdu SI, Brennan MF. Multifactorial analysis of long-term follow-up (more than 5 years) of primary extremity sarcoma. Arch Surg. 1999; 134:190–4. [PubMed: 10025462]
2. Sabolch A, Feng M, Griffith K, Rzasa C, Gadzala L, Feng F, Biermann JS, Chugh R, Ray M, Ben-Josef E. Risk factors for local recurrence and metastasis in soft tissue sarcomas of the extremity. Am J Clin Oncol. 2012; 35:151–7. [PubMed: 21336091]
3. Sadoski C, Suit HD, Rosenberg A, Mankin H, Efird J. Preoperative radiation, surgical margins, and local control of extremity sarcomas of soft tissues. J Surg Oncol. 1993; 52:223–30. [PubMed: 8468983]
4. Pisters PW, Harrison LB, Leung DH, Woodruff JM, Casper ES, Brennan MF. Long-term results of a prospective randomized trial of adjuvant brachytherapy in soft tissue sarcoma. J Clin Oncol. 1996; 14:859–68. [PubMed: 8622034]
5. Olson TP, Harter J, Munoz A, Mahvi DM, Breslin T. Frozen section analysis for intraoperative margin assessment during breast-conserving surgery results in low rates of re-excision and local recurrence. Ann Surg Oncol. 2007; 14:2953–60. [PubMed: 17674109]
6. Valdes EK, Boolbol SK, Cohen JM, Feldman SM. Intra-operative touch preparation cytology; does it have a role in re-excision lumpectomy? Ann Surg Oncol. 2007; 14:1045–50. [PubMed: 17206481]
7. Gareau DS, Jeon H, Nehal KS, Rajadhyaksha M. Rapid screening of cancer margins in tissue with multimodal confocal microscopy. J Surg Res. 2012; 178:533–8. [PubMed: 22721570]
8. Muldoon TJ, Thekkek N, Roblyer D, Maru D, Harpaz N, Potack J, Anandasabapathy S, Richards-Kortum R. Evaluation of quantitative image analysis criteria for the high-resolution microendoscopic detection of neoplasia in Barrett's esophagus. J Biomed Opt. 2010; 15:026027. [PubMed: 20459272]
9. Tanbakuchi AA, Udovich JA, Rouse AR, Hatch KD, Gmitro AF. In vivo imaging of ovarian tissue using a novel confocal microlaparoscope. Am J Obstet Gynecol. 2010; 202:90.e1–9. [PubMed: 19800605]
10. Dobbs JL, Ding H, Benveniste AP, Kuerer HM, Krishnamurthy S, Yang W, Richards-Kortum R. Feasibility of confocal fluorescence microscopy for real-time evaluation of neoplasia in fresh human breast tissue. J Biomed Opt. 2013; 18:106016. [PubMed: 24165742]
11. Boppart SA, Luo W, Marks DL, Singletary KW. Optical coherence tomography: feasibility for basic research and image-guided surgery of breast cancer. Breast Cancer Res Treat. 2004; 84:85–97. [PubMed: 14999139]

12. Nguyen FT, Zysk AM, Chaney EJ, Kotynek JG, Oliphant UJ, Bellafiore FJ, Rowland KM, Johnson PA, Boppart SA. Intraoperative evaluation of breast tumor margins with optical coherence tomography. Cancer Res. 2009; 69:8790–6. [PubMed: 19910294]
13. Mueller JL, Harmany ZT, Mito JK, Kennedy SA, Kim Y, Dodd L, Geradts J, Kirsch DG, Willett RM, Brown JQ, Ramanujam N. Quantitative Segmentation of Fluorescence Microscopy Images of Heterogeneous Tissue: Application to the Detection of Residual Disease in Tumor Margins. PLoS One. 2013; 8:e66198. [PubMed: 23824589]
14. Kirsch DG, Dinulescu DM, Miller JB, Grimm J, Santiago PM, Young NP, Nielsen GP, Quade BJ, Chaber CJ, Schultz CP, Takeuchi O, Bronson RT, et al. A spatially and temporally restricted mouse model of soft tissue sarcoma. Nat Med. 2007; 13:992–7. [PubMed: 17676052]
15. Mito JK, Min HD, Ma Y, Carter JE, Brigman BE, Dodd L, Dankort D, McMahon M, Kirsch DG. Oncogene-dependent control of miRNA biogenesis and metastatic progression in a model of undifferentiated pleomorphic sarcoma. J Pathol. 2013; 229:132–40. [PubMed: 22951975]
16. Mito JK, Ferrer JM, Brigman BE, Lee CL, Dodd RD, Eward WC, Marshall LF, Cuneo KC, Carter JE, Ramasunder S, Kim Y, Lee WD, et al. Intraoperative detection and removal of microscopic residual sarcoma using wide-field imaging. Cancer. 2012; 118:5320–30. [PubMed: 22437667]
17. Muldoon TJ, Pierce MC, Nida DL, Williams MD, Gillenwater A, Richards-Kortum R. Subcellular-resolution molecular imaging within living tissue by fiber microendoscopy. Opt Express. 2007; 15:16413–23. [PubMed: 19550931]
18. Ferguson LR, Denny WA. The genetic toxicology of acridines. Mutat Res. 1991; 258:123–60. [PubMed: 1881402]
19. Krolenko SA, Adamyan SY, Belyaeva TN, Mozhenok TP. Acridine orange accumulation in acid organelles of normal and vacuolated frog skeletal muscle fibres. Cell Biol Int. 2006; 30:933–9. [PubMed: 16895760]
20. Ballard D. Generalizing the Hough Transform to Detect Arbitrary Shapes, vol. 13: Pattern Recognition. 1981:111–22.
21. Cohen C. Image cytometric analysis in pathology. Hum Pathol. 1996; 27:482–93. [PubMed: 8621187]
22. Millot C, Dufer J. Clinical applications of image cytometry to human tumour analysis. Histol Histopathol. 2000; 15:1185–200. [PubMed: 11005244]
23. Eng, J. ROC analysis: Web-based calculator for ROC curves. Vol. 2012. Baltimore: Johns Hopkins University; 2006.
24. Eward WC, Mito JK, Eward CA, Carter JE, Ferrer JM, Kirsch DG, Brigman BE. A novel imaging system permits real-time in vivo tumor bed assessment after resection of naturally occurring sarcomas in dogs. Clin Orthop Relat Res. 2013; 471:834–42. [PubMed: 22972654]
25. Neil MA, Juskaitis R, Wilson T. Method of obtaining optical sectioning by using structured light in a conventional microscope. Opt Lett. 1997; 22:1905–7. [PubMed: 18188403]
26. Fu HL, Mueller JL, Javid MP, Mito JK, Kirsch DG, Ramanujam N, Brown JQ. Optimization of a widefield structured illumination microscope for non-destructive assessment and quantification of nuclear features in tumor margins of a primary mouse model of sarcoma. PLoS One. 2013; 8:e68868. [PubMed: 23894357]
27. Pildes RS, Ramamurthy RS, Vidyasagar D. Effect of triple dye on staphylococcal colonization in the newborn infant. J Pediatr. 1973; 82:987–90. [PubMed: 4702918]
28. Janssen PA, Selwood BL, Dobson SR, Peacock D, Thiessen PN. To dye or not to dye: a randomized, clinical trial of a triple dye/alcohol regime versus dry cord care. Pediatrics. 2003; 111:15–20. [PubMed: 12509548]
29. Browning CH, Gulbransen R, Kennaway EL, Thornton LH. Flavine and brilliant green, powerful antiseptics with low toxicity to the tissues: their use in the treatment of infected wounds. Br Med J. 1917; 1:73–8. [PubMed: 20768444]
30. Shin D, Pierce MC, Gillenwater AM, Williams MD, Richards-Kortum RR. A fiber-optic fluorescence microscope using a consumer-grade digital camera for in vivo cellular imaging. PLoS One. 2010; 5:e11218. [PubMed: 20585636]

31. Tan J, Delaney P, McLaren WJ. Confocal endomicroscopy: a novel imaging technique for in vivo histology of cervical intraepithelial neoplasia. Expert Rev Med Devices. 2007; 4:863–71. [PubMed: 18035951]

32. Tan J, Quinn MA, Pyman JM, Delaney PM, McLaren WJ. Detection of cervical intraepithelial neoplasia in vivo using confocal endomicroscopy. BJOG. 2009; 116:1663–70. [PubMed: 19781048]

33. Aldrich S. Acriflavine hydrochloride: Material Safety Data Sheet. 2015

Novelty and impact

With surgery alone, one-third of patients with soft tissue sarcoma of the extremity will have local recurrence due to microscopic residual disease in the tumor bed. To aid in intraoperative diagnosis, we combined topical acriflavine staining and fluorescence microscopy with appropriate strategies for segmentation and selection of acriflavine positive features, which enables automated detection of microscopic residual sarcoma *in vivo*.

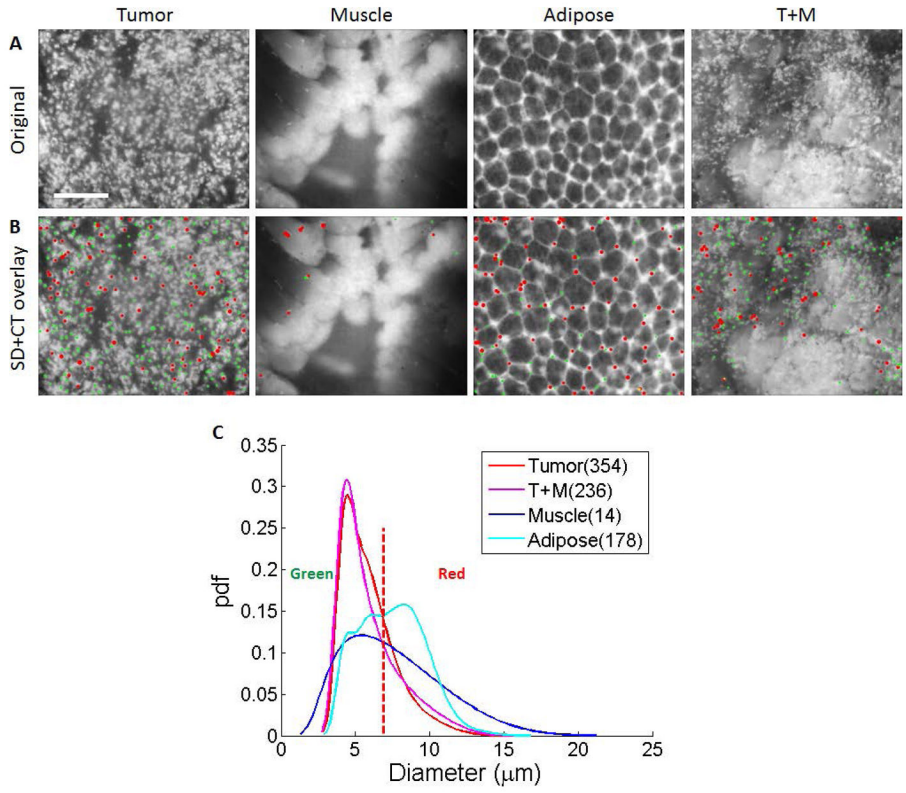

Figure 1.

Application of sparse component analysis (SCA) and circle transform (CT) to representative *ex vivo* images of tumor margins. Tumor, muscle, adipose, and tumor and muscle (T+M) images are shown in (**a**). The original images were analyzed using SCA, and APFs were subsequently quantified with CT. An overlay is shown in (**b**). Scale bar is 200 μm. The probability distribution functions (pdf) of the diameters from the four images are shown in (**c**). The parenthetical values indicate the number of APFs in each image which is synonymous to density, and the vertical dotted red line corresponds to a diameter of 7 μm.

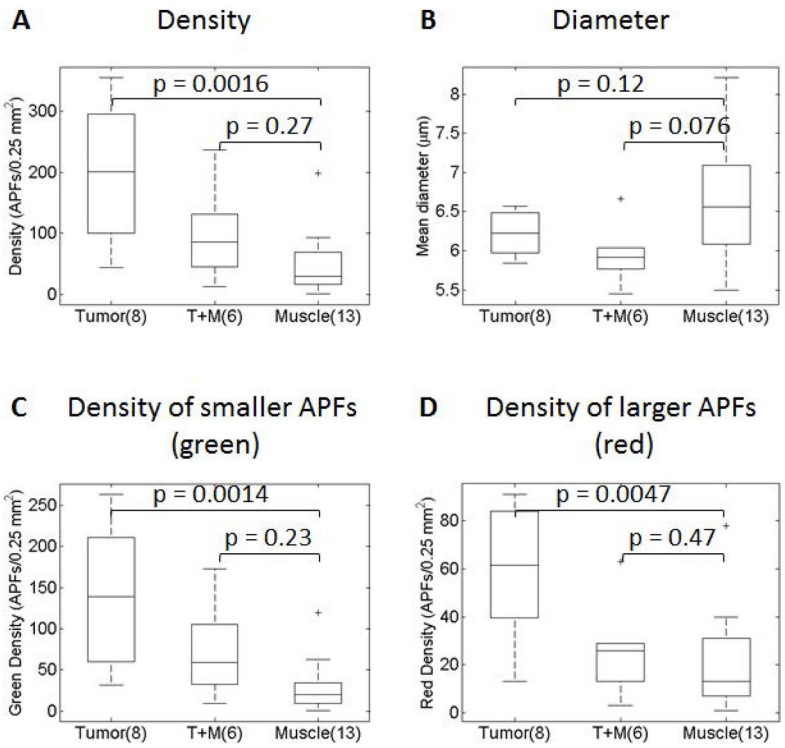

Figure 2.

APF variables calculated for a cohort of *ex vivo* sarcoma margin images. Density and mean diameter were calculated from 8 tumor, 6 tumor + muscle (T+M), and 13 muscle images. For density, boxplots were created for all APFs, the smaller features (green) and the larger features (red) are shown in (**a**), (**c**), and (**d**) respectively. A boxplot of the mean diameter of all APFs is shown in (**b**). P values calculated from Wilcoxon rank sums are shown in each boxplot.

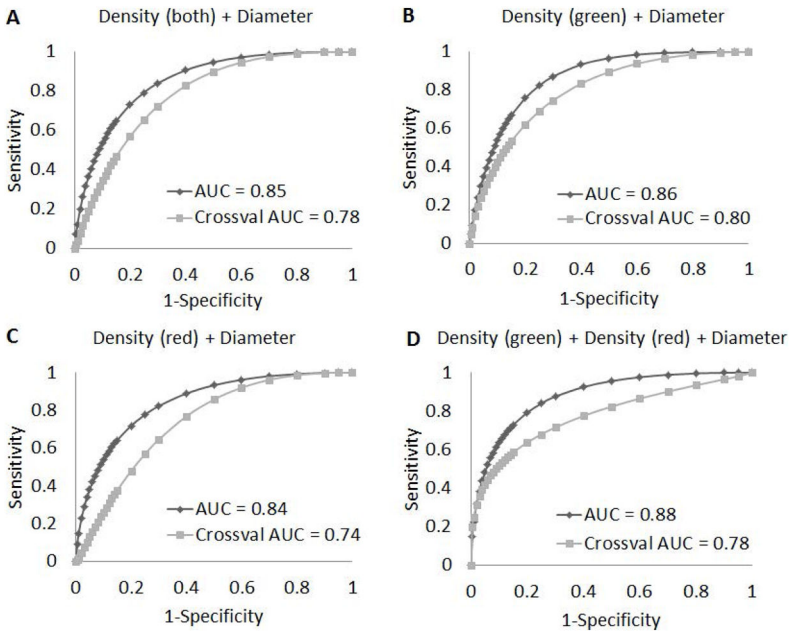

Figure 3.

Multivariate models developed based on *ex vivo* sarcoma margins. The receiver operator curves for all 2 variable and 3 variable combinations are shown in (**a**) – (**d**). Each plot contains curves associated with the original model as well as with cross-validation. The area under the curve (AUC) and the area under the curve associated with the cross-validation (Crossval AUC) are shown on each plot. The density of the smaller features (green), the density of the larger features (red), and the density of all APFs are referred to as Density (green), Density (red), and Density (both) respectively.

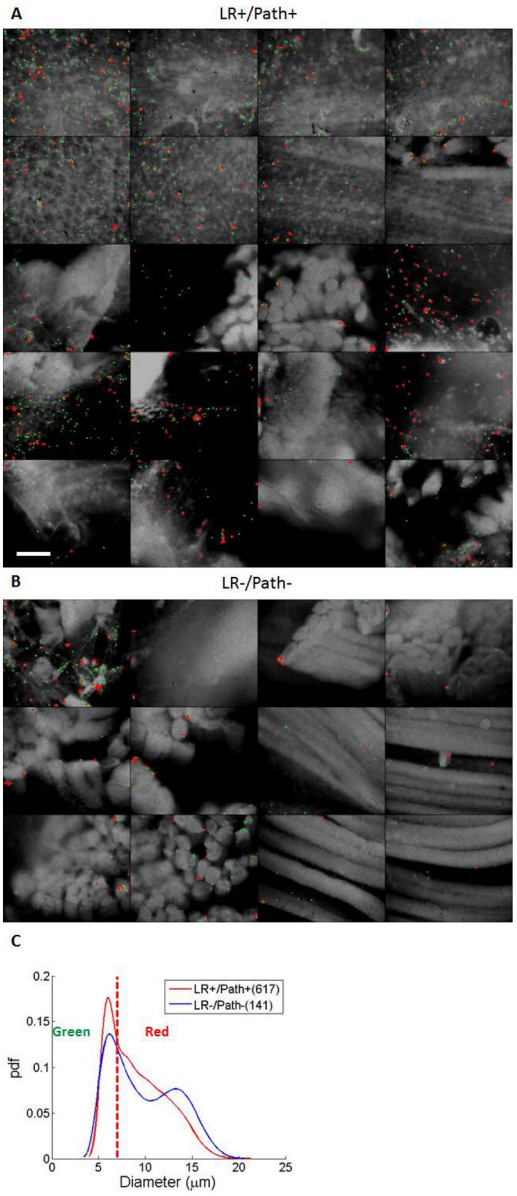

Figure 4.

The application of an algorithm based on sparse component analysis (SCA), and circle transform (CT) applied to representative *in vivo* images from the tumor cavity after resection of the sarcoma. Overlays of a LR+/Path+ and LR−/Path− tumor cavities are shown in (**a**) and (**b**) respectively. The overlays were contrast-stretched in order to enable increased visibility of the false colored APFs. Scale bar is 200 μm. The probability distribution functions (pdf) of the nuclear diameters from the two tumor cavities are shown in (**c**). The parenthetical values indicate the number of APFs in each panel of images, and the vertical dotted red line corresponds to a diameter of 7 μm.

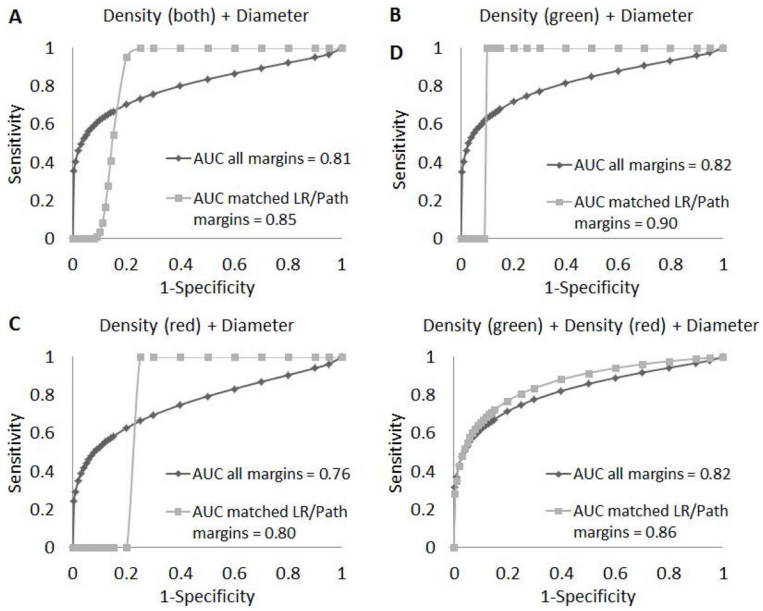

Figure 5.

Multivariate models applied to the *in vivo* images from the tumor cavity predict local recurrence. The receiver operator characteristic curves associated with all of the models shown in Figure 3 are applied here. Each plot contains curves associated with all margins as well as with matching LR+/Path+ and LR−/Path− margins. The area under the curve for all margins (AUC all margins) and the area under the curve for matching LR+/Path+ and LR−/Path− margins (AUC matched LR/Path margins) are shown on each plot.

Table 1

Number of true positives, false negatives, true negatives, and false positives associated with the best performing model

Category	Total	True positives	False negatives	True negatives	False positives
LR+/Path+	2	2	0	0	0
LR+/Path−	5	3	2	0	0
LR+/Path N/A	2	2	0	0	0
LR−/Path−	10	0	0	9	1
LR−/Path+	4	0	0	3	1
LR−/Path N/A	3	0	0	2	1

Abbreviations: LR+/Path+, locally recurred and pathologically positive. LR+/Path−, locally recurred and pathologically negative. LR+/Path N/A, locally recurred and discordant pathology. LR−/Path−, recurrence free and pathologically negative. LR−/Path+, recurrence free and pathologically positive. LR−/Path N/A recurrence free and discordant pathology.